A Method Using Magnetic Eddy Current Testing for Distinguishing ID and OD Defects of Pipelines under Saturation Magnetization

Yue Long [1], Songling Huang [1*], Yang Zheng [2], Shen Wang [1], and Wei Zhao [1]

[1] State Key Laboratory of Power Systems, Dept. of Electrical Engineering
Tsinghua University, Beijing, China
long-y17@mails.tsinghua.edu.cn, huangsling@mail.tsinghua.edu.cn, wangshen@mail.tsinghua.edu.cn, zhaowei@tsinghua.edu.cn

[2] Key Laboratory of Nondestructive Testing and Evaluation of AQSIQ
China Special Equipment Inspection and Research Institute, Beijing, China
zhengyangchina@126.com

Abstract ─ Distinguishing the inside (ID) and outside (OD) defect is an essential problem for the oil and gas pipeline nondestructive testing in engineering. The most widely used solution is to combine a magnetic flux leakage (MFL) section and a second section. For the strong magnetic field environment of the MFL, the second section and the MFL section are usually located at different mechanical positions, which leads to an increase in the length of the pipeline inspection gauge (PIG) and a decrease in the reliability. In this paper, a new impedance measurement method and the concept of the defect impedance angle are proposed to distinguish the ID and OD defects of pipelines under saturation magnetization, which based on the magnetic eddy current testing (MECT). The proposed ID & OD detection method can work with the MFL in the same mechanical position. Meanwhile, the proposed method also has the advantage that the discrimination criteria of the ID and OD defect keeps consistent with the classic eddy current testing (ECT). Furthermore, the robustness and sensitivity of the proposed method are discussed and verified by physical experiments.

Index Terms ─ Impedance measurement, inside and outside defects, magnetic eddy current testing, the defect impedance angle.

I. INTRODUCTION

The pipeline has been widely used in oil and gas transmission projects [1-3]. At present, the total length of oil and gas pipelines has been far more than 10^5 km in China [2,3]. The operating environment of pipelines is relatively harsh, and it is corroded by mud or seawater for a long time, which causes corrosion, and gradually forms defects under the pressure of the transported medium [4,5]. To prevent the occurrence of oil and gas leakage accidents, the pipeline inspection gauge (PIG) is developed for automated non-destructive testing (NDT) of oil and gas pipelines.

The shapes and actual structures of defects for oil and gas pipelines are complex and diverse. There are defects on the inside (ID) or outside (OD) of the pipeline wall [5-8, 10]. In different applications, the impact on the service life of the pipeline, caused by ID or OD defects, is not the same. For marine pipelines, the major cause of the pipeline accident is the ID defect, while for onshore pipelines, OD defects are the main factors threatening the safety of pipelines [7]. In addition, this distinction is essential for pipeline operators to take preventive measures inside or outside the pipeline [8]. Furthermore, it has reference value for pipeline repair work. Therefore, distinguishing the ID and OD defects of the pipeline is essential and meaningful.

For oil and gas pipelines, there are common NDT methods, such as ultrasonic testing (UT) [9], electromagnetic acoustic transducer (EMAT) [10], infrared thermography (IRT) [11], magnetic flux leakage (MFL) [12], eddy current testing (ECT) [5], etc. However, UT requires the couplant, and the inspection speed of UT and EMAT may be lower than the speed of pipeline oil and gas. IRT is more suitable for working outside the pipeline. Therefore, their applications are limited in the actual inspection project. And MFL detection has become the most widely used technology in the field of PIG due to its clear principle, low cost, simple structure and high reliability [13]. However, MFL detection is disabled to distinguish the ID and OD defects [14]. At present, the solution for the pipeline estimation typically uses a '1+1' plus-scheme, in which the MFL detection is selected as the primary unit, mainly responsible for detecting and quantifying the defects. Meanwhile, a second section is set up separately, together with the results of the MFL to distinguish the ID and OD defects. There are usually three options for the

Submitted On: October 24, 2019
Accepted On: July 5, 2020
https://doi.org/10.47037/2020.ACES.J.350916

secondary unit: ECT detection, weak magnetic flux leakage (WMFL) detection, and permanent magnetic field perturbation (PMP) detection.

MFL combined with ECT detection is the most classic method. When the coil passes the defects on the pipeline, the eddy current will be distorted, which can be used to detect defects. Because of the skin effect, it is ID defects that can be detected only by ECT [5]. If the MFL detects a defect while the ECT does not, the defect is an OD defect. Therefore, the MFL and ECT detection results can be added to determine whether it is an ID or OD defect. For example, ROSEN [7] and BARC [8] separated the MFL detection section and the shallow internal corrosion detection section, which is based on ECT. Korea Gas Corporation [15], Hagen Schempf [16] and Albert Teitsma [17] all proposed a comprehensive pipeline inspection robot, in which the detection system consists of the completely independent modules in spatial position: MFL and remote field eddy current testing (RFECT), and other modules.

MFL combined with PMP detection is the most widely used method. PMP detection is that a permanent magnet is surrounded by concentric coils for picking up magnetic field disturbance signals due to defects. The PMP theory and the PMP sensor framework for NDT were first proposed by Yanhua Sun [18]. In 2011, Sun pointed out that the identification of ID and OD defects can be achieved by PMP detection, with the addition of MFL detection [19]. By comparing with MFL detection and ECT detection, Shiwei Liu further elaborated the principle and application of PMP detection [20].

WMFL detection has been developed as one possible method for studying pipeline defects located either ID or OD the structures. Ma Yilai has found that the leakage magnetic field strength of the OD defect in WMFL is much smaller than in MFL. It is possible to distinguish ID and OD defects by combining MFL and WMFL [14]. B. Liu points out that the axial signal of WMFL detection can be used to identify the ID defect [21]. There are many ways to implement the weak magnetic field: some are in the adjacent area outside the closed magnetic circuit composed of NS poles [14], and some directly use the residual magnetism [22].

However, the above three methods have obvious shortcomings. Their principle is to make the ID defects to be detected and OD defects to be not. So, the methods must be added to the MFL detection; otherwise, the OD defects may be missed. Worse, ECT, PMP, and WMFL detection must work under unsaturation magnetization environment, because the saturation magnetization environment of MFL detection will destroy the skin effect of ECT detection and the special magnetic field environment of PMP or WMFL detection. So, the MFL section and other additional detection section are required to be in different mechanical positions. Separating the MFL section from the other detection section will significantly increase the length and costs of the detection system. More seriously, it will reduce its reliability and passing-pipe ability of PIG. How to solve the problem of distinguishing ID and OD defects under saturation magnetization is of great significance.

This paper will propose a detection method based on magnetic eddy current testing (MECT), which can work with MFL in the same mechanical position. That is to say, the proposed MECT method is capable of distinguishing between ID and OD defects in a saturated magnetization environment. It will achieve the fusion of the defect shape detection unit (MFL) and the defect position (ID or OD) detection unit, rather than two units separated by mechanical position. The structure of this paper is shown as following. Firstly, a composite electromagnetic field model is built to analyze the tiny difference between ID and OD defects on the condition of saturation magnetization. Then, one algorithm of impedance measurement based on DFT is proposed. Under the saturation magnetization, the simulation verification and experimental verification of the ID and OD defect distinguishing models are carried out. Based on the experimental results, combined with the characteristics of the ID and OD defects under saturation magnetization, the effectively distinguishing method is discussed.

II. METHODS

A. The composite electromagnetic field model

Since the axes of the coil and the pipe are orthogonal, the two-dimensional (2D) model in the cylindrical coordinate system cannot describe the distribution of the magnetic field in the vicinity of the defect well, so a three-dimensional (3D) model needs to be constructed.

Governing equations

In the conductor region, the oil and gas pipeline is made of ferromagnetic material, and its magnetic permeability μ satisfies the BH curve. In the vicinity of the defects, the different magnetic field strength makes μ not completely uniform. Simultaneously, it is assumed that the conductivity σ does not change substantially with time or space. Therefore, under saturation magnetization, the eddy current governing equation based on the A-V formulations is as follows:

$$\begin{cases} \nabla\times\left(\nabla\times\left(\dfrac{\boldsymbol{A}}{\mu}\right)\right)+\sigma\left(\nabla\dfrac{\partial V}{\partial t}+\dfrac{\partial \boldsymbol{A}}{\partial t}-\boldsymbol{v}\times\nabla\times\boldsymbol{A}\right)=0, \\ \nabla\cdot\sigma\left(\nabla\dfrac{\partial V}{\partial t}+\dfrac{\partial \boldsymbol{A}}{\partial t}-\boldsymbol{v}\times\nabla\times\boldsymbol{A}\right)=0. \end{cases} \tag{1}$$

In the air region, the conductivity σ can be regarded as 0, and the magnetic permeability μ is a constant. The eddy current equation is:

$$\nabla\times\frac{1}{\mu}\nabla\times\boldsymbol{A}=0\,. \tag{2}$$

In addition, the gauge condition of $\boldsymbol{A}$, $\nabla \cdot \boldsymbol{A} = 0$ must be considered. Where V is the time integral electric scalar potential, $\boldsymbol{A}$ is the magnetic vector potential, $\boldsymbol{J}$ is the current density, $\boldsymbol{H}$ is the magnetic field formed by the current in the specimen, $\boldsymbol{B}$ is the magnetic flux density, and $\boldsymbol{v}$ is the speed of PIG.

b. Simulation model

A 3D model is implemented using finite element software-ANSYS Maxwell, which includes PIG and the pipeline with OD or ID defects and shown in Fig. 1 (a). 2D sections of the model are shown as Figs. 1 (b),(c). The integrated probe of PIG includes the coils array for MECT detection and a Hall sensor for MFL detection. The lift-off distance of MFL and MECT is 6.5 mm from the pipe surface, and the diameter and thickness of the pipe are 223 mm and 10 mm. Defects are all cylindrical, 10 mm in diameter and 4 mm in depth. The outer diameter of the coil is 8mm, the height is 4mm, and the number of turns is 300. The pipeline has been saturated magnetized by permanent magnets with the remanence of 1.39 T, and the iron yoke is utilized to constrain magnetic lines between permanent magnets.

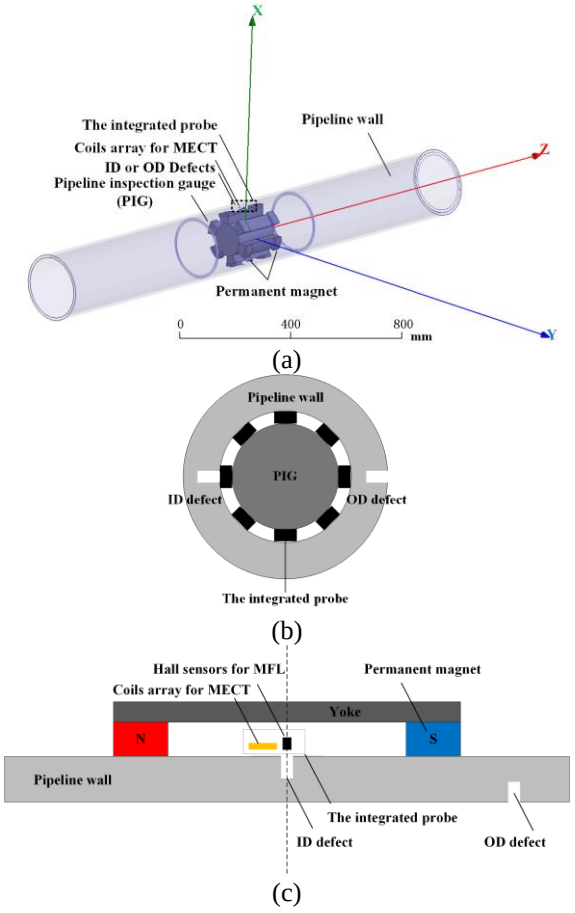

Fig. 1. The finite element model of the composite electromagnetic field model: (a) 3D model, (b) the cross-sectional view, and (c) the cutaway view.

Due to the superposition of the static magnetic field, eddy current field and motion field, a transient magnetic solver has been chosen. The excitation of coils is provided by a dual-arm differential bridge circuit, which at the same time acts as the input of phase sensitive detectors (PSD). The circuit simulation is implemented using Maxwell Circuit Editor. Essentially, it is co-simulation that combines the circuit and electromagnetic field. Furthermore, Dirichlet boundary conditions are applied to the external air model taking into account the characteristics of the composite electromagnetic field.

After inputting the field information, the initial meshing setting is required. To resolve the contradiction between the large volume of the pipe and the small volume of the defect, different grid sizes are selected in different regions. To better simulate the skin effect, the ferromagnetic material has been layered. The last thing to set is the limit of solution error and the number of iterations. In the selection of the model boundary and the initial grid, it is necessary to ensure the setting saturation, that is, when the model boundary is further extended or the initial grid is further subdivided, the result of the solution fluctuates only within an acceptable range.

B. The implementation of impedance measurement

In classical ECT under the condition of unsaturated magnetization, PSD [23-25] and complex impedance analysis [26-29] are the most useful methods to extract valid signal. PSD mainly consists of two parts: the multiplier and the low pass filter, as shown in Fig. 2. Analog multiplier can't satisfy excellent linearity and can't do a good four-quadrant operation. So, this paper has developed the digital PSD by DFT, which is easy to execute on an embedded system.

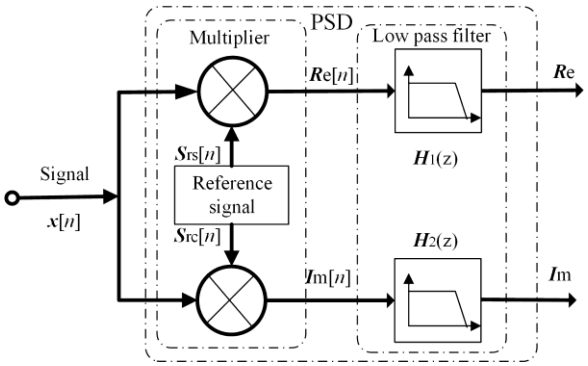

Fig. 2. A classical digital orthogonal PSD.

In a digital PSD, the signal input $x[n]$ can be sampled by ADC and assumed to the equation (3):

$$x[n] = A_0 \sin\left(\frac{2\pi n}{N} + \varphi_0\right), \tag{3}$$

where A_0, φ_0 is the amplitude and phase of the signal. N is the number of samples per cycle, related to frequency

f_0 and sample rate. n is the index of the sequence.

In the field of digital signal processing, the discrete Fourier transform (DFT) is as below:

$$X(k)=\frac{1}{M}\sum_{n=0}^{MN-1}x(n)W_N^{nk},\ W_N=\exp\left(-\mathrm{j}\frac{2\pi}{N}\right), \quad (4)$$

where N is the number of samples per period. M is the number of the period.

Taking k = 1, the conversion between complex exponents and sine and cosine can be obtained:

$$W_N^{\ nk}=\exp\left(-\mathrm{j}\frac{2\pi}{N}nk\right)\Big|_{k=1}=\cos(2\pi\frac{n}{N})+\mathrm{j}\sin(2\pi\frac{n}{N}), \quad (5)$$

where sine and cosine functions are orthogonal, and served as the reference inputs for the orthogonal PSD as the equation (6):

$$S_{\mathrm{rs}}[n]=\sin\left(\frac{2\pi n}{N}\right),\ S_{\mathrm{rc}}[n]=\cos\left(\frac{2\pi n}{N}\right). \quad (6)$$

To simplify the system and increase the speed of calculation, the reference signal $S_{\mathrm{rc}}(n)$ and $S_{\mathrm{rs}}(n)$ are discrete trigonometric function sequence with zero phase and fixed frequency that can be pre-stored in the microprocessor.

Therefore, $x(n)W_N^{nk}$ in equation (3) means that the reference signals $S_{\mathrm{rc}}(n)$ and $S_{\mathrm{rs}}(n)$ are multiplied by input signal $x(n)$. So, $x(n)W_N^{nk}$ can be equivalent to the multiplier shown in Fig. 2. The real and imaginary parts of the output are as follows:

$$R_{\mathrm{e}}(n)=\frac{A_0}{2}\left[\cos(\varphi_0)-\cos\left(\frac{4\pi n}{N}+\varphi_0\right)\right], \quad (7)$$

$$I_{\mathrm{m}}(n)=\frac{A_0}{2}\left[\sin(\varphi_0)+\sin\left(\frac{4\pi n}{N}+\varphi_0\right)\right]. \quad (8)$$

In addition, summation and averaging in equation (3) can be equivalent to the mean filter, which corresponds to the low-pass filter shown in Fig. 2. The filtered real and imaginary parts of the impedance can be obtained:

$$\begin{cases} R_{\mathrm{e}}=\mathrm{R_e}(X(1))\approx\frac{A_0}{2}\cos(\varphi_0), \\ I_{\mathrm{m}}=\mathrm{I_m}(X(1))\approx\frac{A_0}{2}\sin(\varphi_0). \end{cases} \quad (9)$$

The noise reduction ratio (*NRR*) for Mean filter is noticeable:

$$NRR=\frac{1}{MN}. \quad (10)$$

As a result, the digital orthogonal PSD has been designed by DFT. In the microprocessor carried by the PIG, the real-time calculation of the impedance can be realized by calculating the first-order DFT.

III. SIMULATION AND EXPERIMENTS

A. Simulation results

The results of the simulation are shown as Fig. 3, the coils have a certain magnetic concentration capability under the strong magnetic background. When the coils are directly below the non-defective pipeline wall, the magnetic fields induced by the two coils are identical. When the coils are located directly below the ID defect, the magnetic field induced by the coil aligned with the defect is greater than the other one, and the imbalance of the magnetic field induced by the two coils appears. When coils are directly below the OD defect, both coils have the relatively large induced magnetic field, and the induced magnetic field near the defect is also larger, but the imbalance is not as obvious as the situation of the ID defects. The imbalance of the induced magnetic field will cause the imbalance impedance of the two coils, which can be processed and amplified by the differential bridge circuit and PSD.

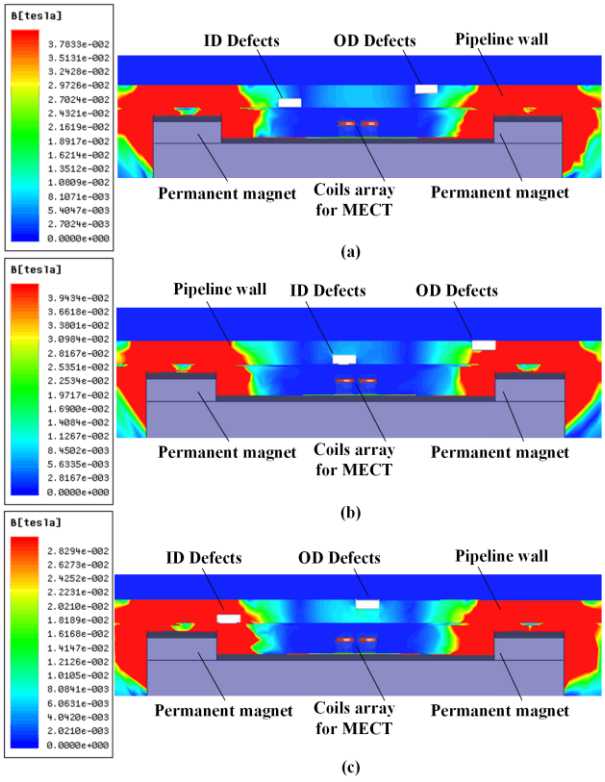

Fig. 3. A 3D finite element model of the composite electromagnetic field model: (a) coils under the pipe wall without defects; (b) coils under the ID defect; (c) coils under the OD defect.

B. The MECT system in physical experiments

The thickness of the pipe wall is 9.80 mm, while the outer diameter is 219 mm. And the size of the defects on specimen are described as Table 1 and Fig. 4 (a).

Table 1: The size of the defects on specimen

The Defects	Diameter	Depth
ID defect	8.22 mm	4.61 mm
OD defect	9.34 mm	4.50 mm

Consistent with the simulation model, the pipeline has been saturated magnetized by permanent magnets with the remanence of 1.39 T. A yoke made of magnetically permeable material is used to constrain the formation of a magnetic circuit to reduce leakage of the air magnetic field. The MFL module and MECT module are integrated together by IC design, as shown in Fig. 4 (b). The excitation of the coil and the pickup of the signal are achieved by a differential bridge circuit on the IC. The algorithm of impedance measurement based on DFT has been implemented by a digital signal proposing (DSP) on board. And the output data are stored in memory via a high speed serial bus.

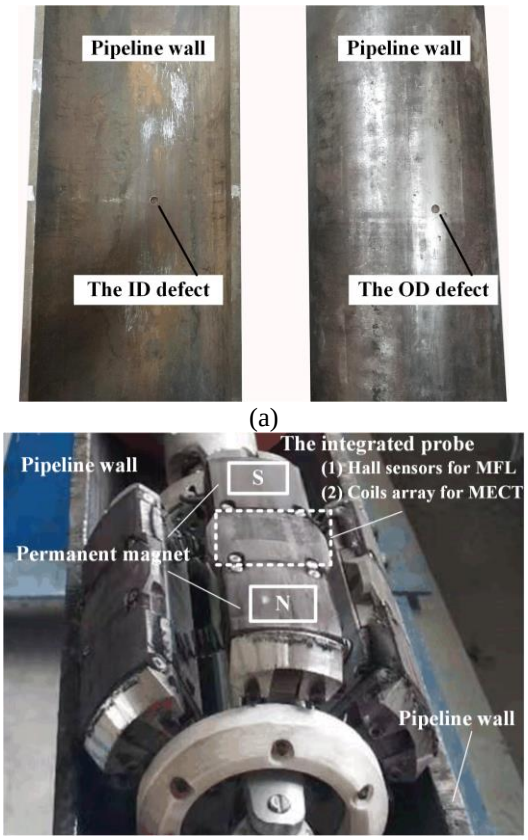

Fig. 4. (a) The semicircular pipeline specimen with an ID defect (left) or OD defect (right); (b) the MECT system.

C. The output of the differential bridge circuit

The output of a differential bridge circuit, the same as the differential input of PSD is shown as Fig. 5. When coils scan through the ID defect, the envelope of the differential signal frequency-modulated by the excitation signal exhibits the characteristics of a double wave crest and a three wave trough, while the wave crest and the wave trough are not prominent when coils scan through the OD defect. For OD and ID defects, both amplitude and phase have changed, and the degree of change is different. However, the amplitudes of the signals of OD and ID defects are similar. Worse, the magnitudes of the effective signal and noise are comparable. And it can be seen from Fig. 5 that the signal-to-noise ratio of a single variable, amplitude or phase, is not large enough to meet industrial applications. Therefore, the subsequent PSD is required to give the result with the combination between the amplitude and phase.

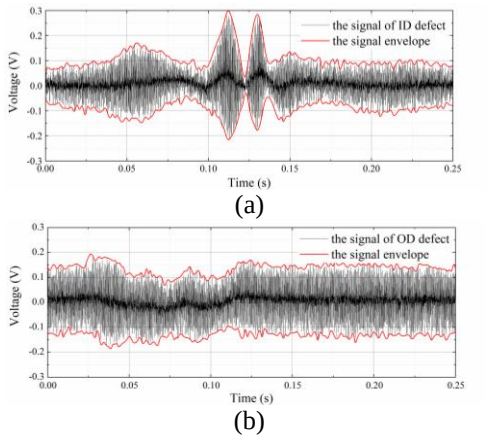

Fig. 5. The output of the differential bridge circuit: (a) when the coils sweep through ID defect; (b) when the coils sweep through OD defect.

D. The measurement result of PSD based on DFT

The driving frequency of the excitation signal is 62.5 kHz, while the sampling rate of the ADC chip is 2 MHz. The number of samples per DFT is 1024. The number of samples per cycle is 32. Each calculation takes 32 cycles.

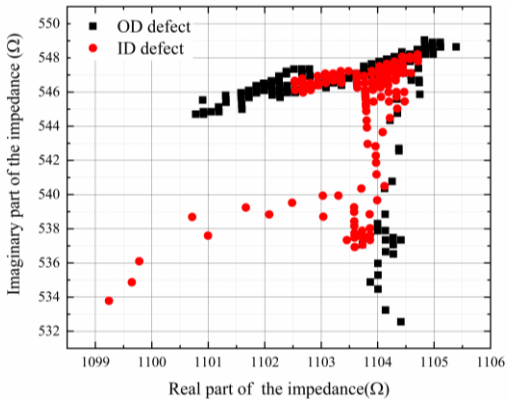

Fig. 6. The complex impedance plane of MECT detection (the pipe wall is under saturation magnetization).

When it is under the condition of saturation magnetization, the impedance feature of typical ID and OD defects is shown in Fig. 6 (a). It can be found that it is ‘T’ shape, not the shape of “8” character in classical

ECT. It can also be found that there are subtle differences included in the general similarity, in local impedance patterns of the ID and OD. When the coil passes ID defects, the main change of the impedance is the decrease of the imaginary part, which is the inductance component. But for OD defects, the resistance decreases drastically, while inductance decreases.

IV. RESULTS AND DISCUSSION

A. The computational domain

To synchronize the variables, such as the maximum, minimum, average of the impedance and so on, a computational domain is defined and can speed up calculations drastically. The computational domain is a certain amount of points near the lowest local inductance. The number of data points that can fully describe the characteristics of the complex impedance plane and maximize the calculation speed is optimal. This paper uses the closed curve of 'T'-type impedance plane as the basis for judging the optimal number of data points in the computational domain.

B. The algorithm based on the defect index for distinguishing the ID and OD defects

In Fig. 6 (a), it can be found that when the coil passes through the ID or OD defects, the inductance will decrease to a similar extent. Therefore, (I_{max} - I_{min}) can be used as a reference value. Meanwhile, (R_{Imin} - R_{ave}) is used to characterize the variation of the resistance of the coil as it passes through the defect. And the defect index is defined in the abbreviated conference version of this paper [30]. Which can use the local data to characterize the graphical features of different defects and analyze the position of defects, whether in the ID or OD:

$$\zeta_O = \frac{R_{I_{min}} - R_{ave}}{I_{max} - I_{min}}, \tag{11}$$

where I_{max} and I_{min} represent the maximum and minimum values of the imaginary part in the computational domain. R_{Imin} represents the real part value corresponding to I_{min}, while R_{ave} represents the real part of the analysis data in the computational domain.

According to the conference version of this paper, the ratio of the defect index of ID and OD is about ten times, which means that the defect index has a strong anti-interference for resolving the defect location.

C. The algorithm based on the defect impedance angle for distinguishing the ID and OD defects

This paper further considers that the ID defect impedance plane is '*T*'-type of italic while the OD is 'T'-type of the normal one. Furthermore, the angle between a horizontal and vertical cross of 'T' or '*T*' is defined as the defect impedance angle (DIA).

The horizontal cross of 'T'-type impedance plane is used as a reference value, which is more statistically significant than (I_{max}-I_{min}). The vertical cross of 'T'-type impedance plane can be characterized by the relationship between the impedance point (R_{Imin}, I_{min}) and the points of the intersection of the horizontal cross and the vertical cross. The point (R_{Imin}, I_{min}) contains information such as the depth and position of the defect, and will not change as the computational domain changes.

For the ID defect in the experiment, the specific algorithm is implemented as follows. First of all, the point (R_{Imin}, I_{min}) is found and equal to (1099.241, 533.787), and the two points of the intersection of the horizontal cross and the vertical cross are (1104.182, 546.688) and (1104.320, 546.690).

Secondly, the reference line can be described by linear regression in the horizontal cross of 'T'-type impedance plane. Using (x, y) to represent the value of the defect impedance plane, the equation of the reference line can be assumed as follows:

$$h_\theta(x) = \theta_0 + \theta_1 x. \tag{12}$$

A cost function $J(\theta_0, \theta_1)$ is set, and θ_0 and θ_1 can be obtained by finding the minimum value of cost function:

$$\underset{\theta_0,\theta_1}{\text{minimize}}\, J(\theta_0,\theta_1) = \frac{1}{2N}\sum_{i=1}^{N}\left(h_\theta(x^{(i)}) - y^{(i)}\right)^2, \tag{13}$$

where N means the number of impedance points on the horizontal cross of 'T'-type impedance plane.

Therefore, the reference line of ID defect is obtained as follow:

$$h(x) = 0.581x - 94.663. \tag{14}$$

Thirdly, combining the point (R_{Imin}, I_{min}) and the two points of the intersection of the horizontal cross and the vertical cross, the line characterizing the defect features can be obtained:

$$g(x) = 2.575x - 2297.1. \tag{15}$$

Lastly, the angle between the reference line and the defect feature line is set to DIA. This angle characterizes the "phase" information of the defect feature. DIA of the ID defect is 38.605°. The reference line, defect feature line and DIA of the ID defect are shown as Fig. 7 (a).

Through the above method, the characteristic value of the OD defect in the experiment can also be calculated. The reference line and the defect feature line of OD defect are shown as Expression (16) and Expression (17), respectively:

$$h(x) = 0.786x - 320.37, \tag{16}$$

$$g(x) = 84.7x - 93011. \tag{17}$$

Therefore, the DIA of the OD defects is 51.149°. The reference line, defect feature line and DIA of the OD defect are shown as Fig. 7 (b).

It can be seen from Fig. 7 that the DIAs of the ID and OD defects are obvious different. The DIA of the ID defect is less than 40°, while the OD defect one is greater than 40°. This result is consistent with the ASME standard for classical ECT. In ASME standard, for thin-walled non-ferromagnetic metal materials, the phase of the ID

defect is specified to 0-40 degrees and the OD one to 40-160 degrees [31]. Therefore, the ID and OD defects of the pipelines under saturation magnetization can be quickly distinguished. The advantage that the discrimination criteria of the ID and OD defect keeps consistent with the classic ECT will bring a lot of benefits, such as subsequent data processing methods for MECT can be compatible with the classic ECT method.

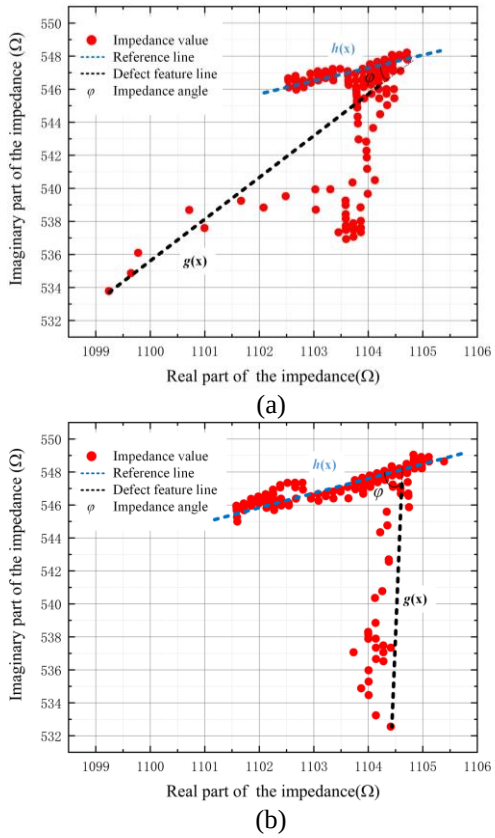

Fig. 7. The reference line, the defect feature line and the DIA: (a) ID defect and (b) OD defect.

D. The robustness of the algorithm based on the defect impedance angle

Compared with the defect index method, this method also has the advantage of being almost unaffected by the size of the computational domain. This method uses statistical methods to obtain the impedance characteristics so that the stability of the results is more robust than the independent method of the defect index method. This conclusion can be demonstrated in Table 2.

Table 2: The defect impedance angle under different computational domains

The Impedance Angle	M = 200	M = 300
ID defect	38.605°	38.545°
OD defect	51.149°	48.229°

M means the number of impedance points in the entire computational domain. Even if the size of the computational domain changes, the DIA remains essentially unchanged. The DIAs of ID defect are always less than 40 degrees, and the OD ones are greater than 40 degrees.

E. The comparison with MFL & ECT combination method

The ID & OD defects have been distinguished successfully by MECT detection. To compare with MECT, the MFL plus ECT detection [7,8] has been conducted on the pipeline specimen in Fig. 4 (a), and the experimental results of the ECT are shown in Fig. 8. It is the standard shape of "8" character as that in classical ECT, which is far different from that in MECT detection.

As shown in Fig. 8, the phase shift method is used to extract the valid signal in ECT. The detection signal is rotated in the complex impedance plane until the noise or OD defect signal coincides with the horizontal axis, so the ID defect signal is automatically separated from the horizontal axis, and it can be detected by determining whether the vertical axis component in the complex impedance plane reaches the threshold. Combined with separate MFL results, ECT can distinguish ID & OD defects. But when the pipe wall is under saturation magnetization, "T" shape in the complex impedance plane cannot be rotated coincide with the x-axis and eliminating the vertical component. Therefore, it is not possible to distinguish ID & OD defects by the amplitude of the Y-axis component. Therefore, ECT section is required to be in a different mechanical position with MFL section, which may significantly increase the costs and reduce the reliability. And MECT overcomes these shortcomings in principle.

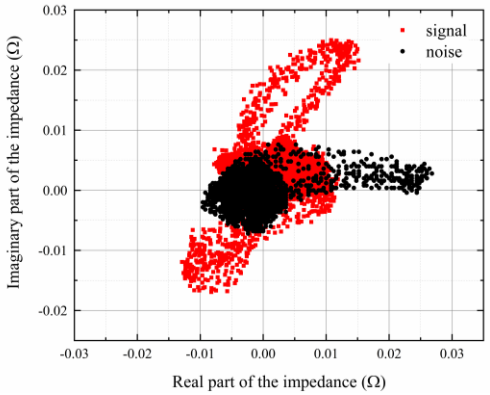

Fig. 8. The complex impedance plane of ECT detection (the specimen is under non-magnetized conditions).

In addition, due to the high permeability of ferromagnetic materials, ECT's ability to inspect pipelines is limited. The skin depth of ECT is as follow:

$$\delta = \frac{1}{\sqrt{f \pi \mu \sigma}}, \quad (18)$$

where σ and μ are the conductivity and permeability of the pipeline, f is the frequency of the excitation current in ECT. The excitation frequency f is generally 1-100 kHz, so the skin depth δ on the ferromagnetic pipeline is generally about 1 mm [28,29,32], which is much smaller than the thickness of the oil and gas pipeline wall. When the pipe wall is under saturation magnetization, the permeability μ reduces several-hundred times, and the skin depth δ will increase ten times in MECT, which covers the range of pipe thickness.

F. The sensitivity of MECT detection

Since the excitation circuit and dual-arm differential bridge circuit of MECT are analog circuits, and followed by PSD with extremely high signal-to-noise ratio, the sensitivity is mainly determined by the accuracy of the ADC and the circuit threshold of the PSD circuit.

For NDT of pipelines, the sensitivity of the inspection system is usually evaluated by the percentage of the defect depth in the thickness of the pipeline wall. To describe the sensitivity, the paper sets two extreme experiments. The paper selects a relatively shallow ID defect to test whether MECT is not sensitive enough to identify the defect and produce a missed judgment. At the same time, the paper also selected a relatively deep OD defect to test whether MECT would misjudge it as an ID defect. The geometric parameters of these two defects are shown in Table 3. And the thickness of the pipe wall D is 8 mm. The depth of ID defects is the minimum depth that needs to be detected in routine engineering inspection. The depth of the OD defect has exceeded half the thickness of the pipe wall, which is a fatal threat to the safe transmission of oil and gas, and it is very easy to be mistakenly identified as an ID defect.

The calculated impedance angle is also shown in Table 3, and it can be found that even in the low signal-to-noise ratio case (shallow ID defect or deep OD defect), MECT can still distinguish between ID and OD defects.

Table 3: The size of the defects on specimen

Defects	Diameter	Depth	Impedance Angle
ID	11.67 mm	0.135 D	30.417°
OD	8.10 mm	0.718 D	69.162°

V. CONCLUSION

Based on the problem that under the saturation magnetized condition, the MFL detection and classical ECT detection and so on cannot distinguish the ID and OD defects. This paper firstly builds a composite electromagnetic field model to analyze the infinitesimal difference between ID and OD defects on the condition of saturation magnetization by the MECT method. The implementation of impedance measurement based on DFT has been proposed to achieve MECT detection. ANSYS simulation model verified the tiny difference between ID and OD defects. The physical experiment obtained the time domain waveform and impedance plane of the coil impedance. It has been found that the impedance plane of MECT under saturation magnetization showed a 'T' shape instead of the '8' shape of the ECT under unsaturation magnetization. Furthermore, the definition and calculation method of the DIA of MECT under saturation magnetization are proposed, and the conclusion that is consistent with ECT is obtained: an ID defect with an impedance angle less than 40 degrees and an OD defect with an impedance angle greater than 40 degrees.

The experiment proves that the method has stronger robustness because it uses the statistical characteristics of the defect impedance, which has a promising significance of engineering application. The MECT method based on impedance angle has high sensitivity and can still distinguish between ID and OD defects very well in the low signal-to-noise ratio case.

Combining MECT with MFL detection, the location (in the ID or OD) and the type of defect can both be solved, which provides a comprehensive solution for the pipeline estimation. MECT can work with the MFL in the same position, which will reduce the mechanical length of the PIG and improve reliability.

ACKNOWLEDGMENT

This research was supported by the National Natural Science Foundation of China (NSFC) (No. 51677093) and the National Key Scientific Instrument Development Projects (No. 2013YQ140505).

REFERENCES

[1] J. Feng, F. Li, S. Lu, J. Liu, and D. Ma, "Injurious or non-injurious defect identification from MFL images in pipeline inspection using convolutional neural network," *IEEE Transactions on Instrumentation and Measurement*, pp. 1-10, 2017.

[2] X. Chen, Z. Wu, W. Chen, R. Kang, X. He, and Y. Miao, "Selection of key indicators for reputation loss in oil and gas pipeline failure event," *Engineering Failure Analysis*, vol. 99, pp. 69-84, 2019.

[3] J. Zhou, J. Peng, G. Liang, and T. Deng, "Layout optimization of tree-tree gas pipeline network," *Journal of Petroleum Science and Engineering*, vol. 173, pp. 666-680, 2019.

[4] A. Cosham, P. Hopkins, and K. A. Macdonald, "Best practice for the assessment of defects in pipelines–Corrosion," *Engineering Failure Analysis*, vol. 14, no. 7, pp. 1245-1265, 2007.

[5] J. Yin, M. Lu, and D. Pineda, "Full-signature real-time corrosion detection of underground casing pipes," *IEEE Transactions on Instrumentation and*

Measurement, vol. 49, pp. 120-128, 2000.

[6] R. Palanisamy and W. Lord, "Prediction of eddy current probe signal trajectories," *IEEE Transactions on Magnetics*, vol. 16, no. 5, pp. 1083-1085, 1980.

[7] T. Beuker and B. Brown, "Monitoring of top of line corrosion with eddy current technology combined with magnetic flux leakage method," *Corrosion 2010 NACE International*, 2010.

[8] D. Mukherjee, S. G. Manral, S. Chand, S. Dhage, S. Bahuguna, S. Saha, S. K. Lahiri, S. Mukhopadhyay, and A. Kumar, "Development of secondary sensor system based on eddy current technology for in-line inspection tool," *Barc Newsletter*, 2013.

[9] W. T. Peter and X. Wang, "Characterization of pipeline defect in guided-waves based inspection through matching pursuit with the optimized dictionary," *NDT & E International*, vol. 54, pp. 171-182, 2013.

[10] Z. Wang, S. Huang, Q. Wang, S. Wang, and W. Zhao, "Time of flight extraction of dispersive Lamb wave by ridge analysis," *In 2018 International Applied Computational Electromagnetics Society Symposium-China (ACES), IEEE*, pp. 1-2, 2018.

[11] S. Bagavathiappan, B. B. Lahiri, T. Saravanan, J. Philip, and T. Jayakumar, "Infrared thermography for condition monitoring - A review," *Infrared Physics & Technology*, vol. 60, no. 60, pp. 35-55, 2013.

[12] J. Chen, "3-D defect profile reconstruction from magnetic flux leakage signals in pipeline inspection using a hybrid inversion method," *Applied Computational Electromagnetics Society Journal*, vol. 32, no. 3, pp. 268-274, 2017.

[13] Y. Shi, C. Zhang, R. Li, M. Cai, and G. Jia, "Theory and application of magnetic flux leakage pipeline detection," *Sensors*, vol. 15, pp. 31036-31055, 2015.

[14] M. Yilai and L. Li, "Research on internal and external defect identification of drill pipe based on weak magnetic inspection," *Insight: Non-Destructive Testing & Condition Monitoring*, vol. 56, no. 1, pp. 31-34, 2014.

[15] D.-K. Kim, H.-R. Yoo, S.-H. Cho, S.-J. Koo, D.-K. Kim, J.-S. Yoo, and Y.-W. Rho, "Inspection of unpiggable natural gas pipelines using in-pipe robot," *International Conference on Advanced Engineering Theory and Applications*, pp. 364-373, 2016.

[16] H. Schempf, E. Mutschler, A. Gavaert, G. Skoptsov, and W. Crowley, "Visual and nondestructive evaluation inspection of live gas mains using the Explorer™ family of pipe robots," *Journal of Field Robotics*, vol. 27, no. 3, pp. 217-249, 2010.

[17] A. Teitsma, "Remote field eddy current inspection of unpiggable pipelines," *Office of Scientific & Technical Information Technical Reports*, 2004.

[18] Y. Sun, Y. Kang, and C. Qiu, "A permanent magnetic perturbation testing sensor," *Sensors & Actuators A: Physical*, vol. 155, no. 2, pp. 226-232, 2009.

[19] Y. Sun, Y. Kang, and C. Qiu, "A new NDT method based on permanent magnetic field perturbation," *NDT & E International*, vol. 44, no. 1, pp. 1-7, 2011.

[20] S. Liu, Y. Sun, M. Gu, C. Liu, L. He, and Y. Kang, "Review and analysis of three representative electromagnetic NDT methods," *Insight*, vol. 59, no. 4, pp. 175-183, 2017.

[21] B. Liu, Y. Cao, H. Zhang, Y. R. Lin, W. R. Sun, and B. Xu, "Weak magnetic flux leakage: A possible method for studying pipeline defects located either inside or outside the structures," *NDT & E International*, vol. 74, pp. 81-86, 2015.

[22] V. Babbar and L. Clapham, "Residual magnetic flux leakage: a possible tool for studying pipeline defects," *Journal of Nondestructive Evaluation*, vol. 22, no. 4, pp. 117-125, 2003.

[23] X. Ren and S. Liu, "Experimental study of phase sensitive detection technique in ECT system," *In 2014 International Conference on Machine Learning and Cybernetics, IEEE*, vol. 1, pp. 121-125, 2014.

[24] D. L. Birx and S. J. Pipenberg, "A complex mapping network for phase sensitive classification," *IEEE Transactions on Neural Networks*, vol. 4, no. 1, pp. 127-135, 1993.

[25] L. S. Obrutsky, V. S. Cecco, S. P. Sullivan, and D. Humphrey, "Transmit receive eddy current probes for circumferential cracks in heat exchanger tubes," *Materials Evaluation*, vol. 54, no. 1, pp. 93-98, 1996.

[26] F. Lingvall and T. Stepinski, "Automatic detecting and classifying defects during eddy current inspection of riveted lap-joints," *NDT & E International*, vol. 33, no. 1, pp. 47-55, 2000.

[27] J. M. Prince and B. P. Hildebrand, "Low-frequency electromagnetic (eddy-current) holography for imaging in conductors," *Applied Optics*, vol. 32, no. 26, pp. 4960-4971, 1993.

[28] B. Helifa, M. Féliachi, I. K. Lefkaier, B. Fouad, A. Zaoui, and N. Lagraa, "Characterization of surface cracks using eddy current NDT simulation by 3D-FEM and inversion by neural network," *In Workshop Problem*, vol. 15, pp. 10, 2016.

[29] H. A. Sabbagh, R. K. Murphy, E. H. Sabbagh, J. Aldrin, J. Knopp, and M. Blodgett, "Computational electromagnetics and model-based inversion: A modern paradigm for eddy-current nondestructive evaluation," *Applied Computational Electromag-*

netics Society Journal, vol. 24, no. 6, pp. 533-540, 2009.

[30] Y. Long, S. Huang, J. Yu, W. Zhao, and S. Wang, "A method of distinguishing the ID and OD defect of the pipe under saturation magnetization," *2018 International Applied Computational Electromagnetics Society Symposium - China (ACES)*, pp. 1-2, 2018.

[31] D. H. Hur, M. S. Choi, H.-S. Shim, D. H. Lee, and O. Yoo, "Influence of signal-to-noise ratio on eddy current signals of cracks in steam generator tubes," *Nuclear Engineering and Technology*, vol. 46, no. 6, pp. 883-888, 2014.

[32] G. Rubinacci, A. Tamburrino, and S. Ventre, "Eddy current imaging of surface breaking defects by using monotonicity based methods," *Applied Computational Electromagnetics Society Journal*, vol. 23, no. 1, pp. 46-52, 2008.

Yue Long received the B.S. degree from School of Automation Science and Electrical Engineering, Beihang University, Beijing, China, in 2017. He is currently pursuing a Ph.D. degree within the Department of Electrical Engineering, Tsinghua University. His major research interests include electromagnetic measurement and nondestructive evaluation.

Songling Huang received the bachelor's degree in Automatic Control Engineering from Southeast University, Nanjing, China, in 1991, and the Ph.D. degree in Nuclear Application Technology from Tsinghua University, Beijing, China, in 2001.

He is currently a Professor within the Department of Electrical Engineering, Tsinghua University. His research interests include nondestructive evaluation and instrument techniques.

Yang Zheng received his B.Sc. degree in Mechanical Engineering and Automation from BeiHang University in 2007 and Ph.D. degree in Mechanical Engineering from Beijing University of Technology in 2012.

Now He works as a Research Fellow in China Special Equipment Inspection and Research Institute. He works on the non-destructive testing and evaluation techniques, mainly including inspection methods study, instruments development and standards development. His current research interests include electromagnetic acoustic transducers and material magnetic testing methods.

Shen Wang received the bachelor's and Ph.D. degrees in Electrical Engineering from Tsinghua University, Beijing, China, in 2002 and 2008, respectively.

He is currently an Associate Professor within the Department of Electrical Engineering, Tsinghua University. His research interests include nondestructive testing and evaluation, and virtual instrumentation.

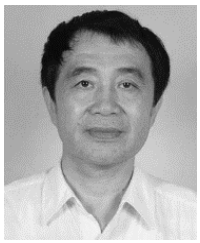

Wei Zhao received the bachelor's degree in Electrical Engineering from Tsinghua University, Beijing, China, in 1982, and the Ph.D. degree from the Moscow Power Engineering Institute Technical University, Moscow, Russia, in 1991.

He is currently a Professor within the Department of Electrical Engineering, Tsinghua University. His research interests include modern electromagnetic measurement and instrument techniques.